Journal of Polymers and the Environment (2018) 26:4158–4167
https://doi.org/10.1007/s10924-018-1286-4

ORIGINAL PAPER

The Investigation of the Toughening Mechanism of PHBV/PBAT with a Novel Hyperbranched Ethylenediamine Triazine Polymer Based Modifier: The Formation of the Transition Layer and the Microcrosslinking Structure

Yujuan Jin[1] · Ee Wang[1] · Yunxuan Weng[1] · Shuang Men[2] · Yuping Dong[3] · Yangyang Sima[1] · Zhigang Huang[1]

Published online: 31 July 2018

Abstract
A new type of designed hyperbranched ethylenediamine trazine polymer (HBETP) is successfully synthesized and characterized based upon NMR and GPC. The prepared HBETP is used to modify the poly(hydroxybutyrate-co-hydroxyvalerate) (PHBV)/poly(butylene adipate-co-terephthalate) (PBAT) blends. The effect of HBETP on the microstructure, mechanical properties and thermal properties of the blends is studied. The results indicate that upon addition of 1.0 wt% of HBETP, the impact strength of the PHBV/PBAT blends is increased by 47.1%; ΔT_g of the blends decreases from 53.2 to 49.9 °C. These results, together with the morphology analysis of the fractured surface of the blends, conclude the formation of the transition layer between PHBV and PBAT. Also, the XRD result shows that the addition of HBETP can limit the growth of the PHBV crystals and causes the decrease of both the crystallinity and the grain crystalline size. The DSC result demonstrates that the addition of HBETP mainly affects the crystallization of the HB-HV binary eutectic region within PHBV. The mechanism of PHBV/PBAT toughening is due to the formation of the strong physical hydrogen bonding and the chemical micro-crosslinking between HBETP and PHBV/PBAT, which is proposed based on XPS characterization.

Keywords Transition layer · Micro-crosslinking · HBETP · PHBV/PBAT · Toughness

Introduction

Polymer materials have found increasingly widespread applications over the past several decades. However, most of the existing synthetic polymers are non-degradable. Their disposal creates serious white pollution. Also, the ever growth of the cost of petroleum products has been of great concerns. Taking into account the reality that petroleum resources are in great shortage, many attempts have been conducted aiming to replace petroleum products by other sustainable resources. Thus, in recent years, bio-based and biodegradable polymers have attracted expanded attentions which can effectively reduce the environmental pollution and the consuming of nonrenewable sources, i.e. petroleum and gas products [1–6].

Poly(hydroxybutyrate-co-hydroxyvalerate) (PHBV) is a type of typical bio-based and biodegradable polymer produced in nature by microorganism under the condition of non-equilibrium status [7, 8]. It is formed as intracellular carbon sources and energy reserve in organism. It has found potential applications in packaging, automotive, biomedicine and agriculture, ascribing to its biodegradability, biocompatibility, piezoelectricity and optical activity. However, PHBV has some intrinsic drawbacks which restrict its applications, such as high hardness and fragility, high cost, poor impact resistance, slow crystallization rate and extreme instability in molten state. Meanwhile, the thermal degradation temperature of PHBV is found closed to its melting temperature. All these disadvantages have made the processing of PHBV

✉ Yujuan Jin
jinyujuan@th.btbu.edu.cn

1 School of Materials and Mechanical Engineering, Beijing Technology and Business University, Beijing 100048, People's Republic of China

2 School of Material Science and Engineering, Shenyang Ligong University, Shenyang 110159, People's Republic of China

3 School of Material Science and Engineering, Beijing Institute of Technology, Beijing 100081, People's Republic of China

difficult. In order to solve such a problem, blending modification is an effective method commonly employed [9–18].

Poly(butylene adipate-co-terephthalate) (PBAT) is also a kind of full-biodegradable polymer which integrates the flexibility of PBA chains with higher thermal resistance, and PBT chains which possess high impact resistance [19, 20]. The blending modification of PHBV and PBAT can enhance the general performances of the material, and ensure the biodegradability of the blends. However, the poor compatibility between PHBV and PBAT directly leads to a dramatic decrease in the mechanical property of the PHBV/PBAT blends [12–15]. In order to improve the mechanical properties of the PHBV/PBAT blends, various types of compatibilizers have been added to the blends. Pawar et al. reported the effect of graphene nanosheets and vermiculite on tensile properties of the PHBV/PBAT composites [12]. It was found that upon addition of graphene, the composites showed remarkable enhancement in tensile strength. Nagarajan et al. studied the effect of pMDI as a compatibilizer on the impact strength of the PHBV/PBAT blends [13]. It concluded that when the concentration of pMDI was 1 phr, the impact strength of the composite increased by 102%, compared to that containing 30 wt% of switchgrass. Javadi et al. demonstrated the effect of recycled wood fiber (RWF) on the mechanical properties of the PHBV/PBAT blends [15]. It reported that the storage modulus of the PHBV/PBAT blends increased specifically upon addition of 10 wt% of RWF, when compared to that of the neat PHBV/PBAT blends.

Hyperbranched polymers (HBP), which are polymerized with polyfunctional monomers, represent a novel polymer form developed over the past three decades. Compared with linear polymers, HBPs have many unique advantages, such as high degree of branching, low probability of molecular chain entanglement, low viscosity and low crystallinity. There are also plenty of active terminal functional groups within HBP, which enable certain types of hydrogen bonding and/or chemical reactions between HBP and other polymers. On the other hand, compared with micro-molecular modifiers, HBPs are more stable in blends because they are difficult to be separated and migrate, which makes themselves more suitable in the application of packaging materials, e.g. food packaging. As a result, HBPs are widely used as modifiers in many investigations. It has been found that the strong interactions between HBP and blended polymers could influence the properties of polymeric blends, such as glass transition temperature (T_g), melting point, crystallinity, and surface energy [21–30].

In this study, a new type of hyperbranched ethylenediamine trazine polymer (HBETP) was synthesized by one-step method and was used as the compatibilizer for the PHBV/PBAT blends. The effect of the addition of HBTEP on the microstructure, mechanical properties and thermal properties of the PHBV/PBAT blends was demonstrated. The toughening mechanism is discussed in detail. It proposes that upon addition of HBETP, both the physical hydrogen bonding effect and the chemical microcrosslinking occurred.

Materials and Methods

Materials

Ethylene-diamine (analytical reagent) was purchased from Beijing chemical plant, Beijing, China. Cyanuric chloride (analytical reagent), sodium carbonate (analytical reagent), and acetone (analytical reagent) were purchased from Beijing Chemical Reagent Company, Beijing, China. PHBV (Technical Pure, $\overline{M_w} = 3.0 \times 10^5$ g mol^{-1}, the molar content of HV is 3%) (Y1000P) was purchased from Ningbo Tian'an Biological Materials Co., Ltd., Ningbo, Zhejiang Province, China, and the molecular structure of PHBV is shown in Fig. 1. PBAT (TP, $\overline{M_w} = 1.2 \times 10^5$ g mol^{-1}, the molar content of AT is 55%) (Ecoworld®) was purchased from Jinhui Zhaolong High Technology Co., Ltd., Xiaoyi, Shanxi Province, P. R. China.

Synthesis of HBETP

73.8 g Cyanuric chloride and 700 mL acetone were mixed together and added into a 1000 mL three-necked glass flask. 48 g ethylene diamine and 25.4 g sodium carbonate were dissolved in 250 mL deionized water at 80 °C. The aqueous solution was then cooled down to room temperature and added to the reaction system by dropwise. The mixture was stirred at room temperature. During the polymerization, a large number of bubbles and white particles were observed in the solution. The reaction was carried out for 7 h. The reaction mixture was filtered and the product was rinsed with hot deionized water and acetone three times separately. The target product, HBTEP, was dried for 48 h in a vacuum oven at 90 °C to yield a white solid with the yield of 96.3%. The structure of the synthesized HBTEP is shown in Fig. 2.

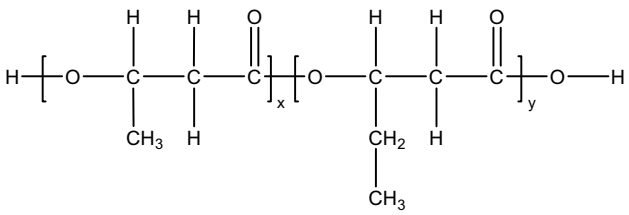

Fig. 1 Molecular structure of PHBV

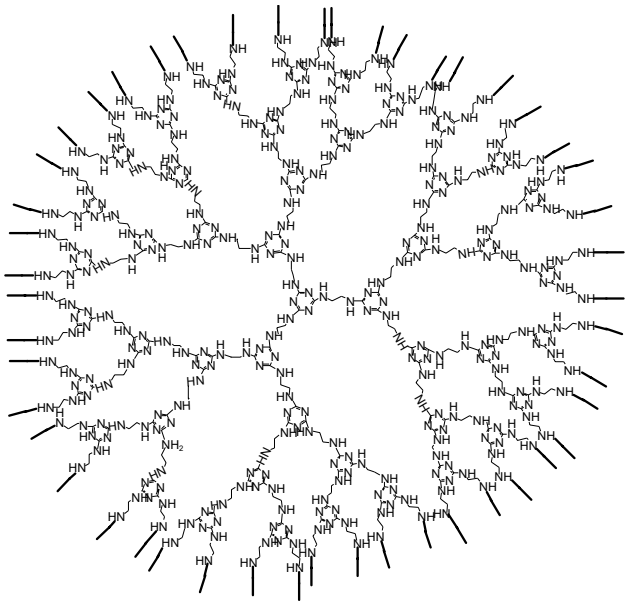

Fig. 2 Schematic diagram of HBTEP molecular structure

Characterization of HBETP

Characterization of HBETP by Nuclear Magnetic Resonance

^{1}H and ^{13}C nuclear magnetic resonance (NMR) spectra were recorded using a Bruker Advance 400 spectrometer (Agilent NMR Magnet) at 400 and 100 MHz respectively, as solutions dissolved in DMSO-d_6 at room temperature.

Characterization of HBETP by Gel Permeation Chromatography

Gel permeation chromatography (GPC) (DAWN HELEOS-II, Wyatt, USA) was carried out using dimethylsulfoxide as the solvent. Concentration is 1 mg mL^{-1}. Calibration was performed using polystyrene standards.

PHBV/PBAT/HBETP Blends Preparation

700 g PHBV, 300 g PBAT and a certain amount of HBETP (0, 5, 10 and 20 g, respectively) were placed in a vacuum oven and dried for 12 h at 90 °C. The parameters of the twin-screw extruder (CTE-35, Koblon Koya Machinery Co., Ltd., Nanjing, Jiangsu Province, China.) were set at 175, 175, 180, 180, 180 and 175 °C (from one area to six area), all ingredients were melt blended by a twin-screw extruder. The blends were then cooled down to room temperature before pelletized by a pelletizer. The mixing temperature was set to 152 °C, and the injection pressure was 4 MPa. Standard splines were made through an injection molding machine (TY-400, Hangzhou Dayu Machinery Co., Ltd., Hangzhou, Zhejiang Province, PR China).

Characterization of the PHBV/PBAT Blends

Mechanical Properties

Tensile strength of the blends was tested by a computer-controlled electronic universal testing machine (CMT6104, MTS Industry System Co., Ltd., Shenzhen, Guangdong Province, PR China) according to GB/T 1040.2-2006 Standard. The tensile rate was chosen to be 5 mm min^{-1}. The size of the spline was determined according to the GB/T 1040.2-2006 standard: dumbbell shaped spline, L = 150 mm, d = 4 mm.

Impact strength was tested by an electronic Izod impact testing machine (XJUD-5.5, Chengde Jinjian Testing Instrument Co., Ltd., Chengde, Hebei Province, PR China) according to GB/T 1843-2008 standard (ISO180:2000). The size of the A-type notched spline was determined according the GB/T 1843-2008 standard (ISO180:2000): 80 mm × 10 mm × 4 mm. The impact energy of the pendulum was 4 J.

DMA

The dynamic mechanical analyzer (DMA) (242C, NETZSCH, Germany) of the PHBV/PBAT blends with various HBTEP contents were measured under liquid nitrogen atmosphere. The sample dimensions were approximately 10 mm × 30 mm × 2 mm. The parameters of dynamic mechanical analysis for the samples were set as follows: temperature range, − 80 to 70 °C; heating rate, 3 °C min^{-1}; frequency, 5 Hz.

X-Ray Photoelectron Spectroscopy

All X-ray photoelectron spectroscopy (XPS) spectra were recorded using a PHI Quantera II spectrometer employing a focused, monochromated Al Kα source ($h\nu = 1486.6$ eV), hybrid (magnetic/electrostatic) optics, hemispherical analyser and a multi-channel plate and delay line detector (DLD) with a X-ray incident angle of 30° and a collection angle, θ, of 0° (both relative to the surface normal). The analysed area was 100 μm × 100 μm, and 16 different spots of each sample were analysed. All XPS measurements were conducted at room temperature.

For data interpretation, a spline linear background subtraction was used. Peaks were fitted using GL(30) lineshapes; a combination of a Gaussian (70%) and Lorentzian (30%) [31]. All XP spectra were charge corrected by setting the measured binding energy of the $C_{aliphatic}$ 1s to 285.0 eV.

XRD

X-ray diffraction (XRD) (D8 advance, Haake, Germany) patterns were obtained at room temperature. The scanning range was 5°–80° at a rate of 4°/min. The sample dimensions were approximately 30 mm × 30 mm × 2 mm.

DSC

The differential scanning calorimeter (DSC) (Q100, TA, USA) of the PHBV/PBAT blends with various HBTEP contents were measured under the protection of nitrogen gas. The sample (5.0–10.0 mg) was heated from room temperature to 200 °C, pre-annealed at 200 °C for 3 min, followed by cooling to − 70 °C at 20 °C min^{-1} and then reheated to 200 °C at 10 °C min^{-1}.

Morphology of the Fractured Surface

The morphology of the fractured surface of the impact sample was observed under scanning electron microscopy (SEM) (QUATA250, FEI, USA). Before SEM, gold spraying was performed with a working voltage of 15 kV.

Results and Discussion

NMR Analysis of HBETP

Figure 3a demonstrates the ^{1}H NMR spectrum of HBETP. As expected, there are three proton signals showing chemical shifts at 2.05, 3.45 and 9.13 ppm, respectively. The signal at 2.05 originates from the proton of the terminal amino group (–NH_2). The other two signals represent the protons of the –CH_2– and –NH– groups, respectively. In ^{1}C NMR spectrum, as shown in Fig. 3b, the peak at 39.94 ppm is assigned to –CH_2– group; signals ranging from 166 to 169 ppm can be attributed to carbons within triazine structure. These results conclude that the target product, HBETP, has been successfully prepared.

GPC Analysis of HBETP

The measured number-average molecular weight of HBETP is 2.05×10^4. It is calculated that the molecular weight of the molecular chain segment of HBETP is 194. The molecular weight of the n-th generation HBETP is $252 + 194 \times 3 \times (2^{n-1} - 1)$. Therefore, it is calculated that n = 6, indicating that the generated HBETP contains 96 terminal amino groups.

Mechanical Properties Analysis of PHBV/PBAT

The data of tensile strength and impact strength for the blends with different contents of HBTEP are given in Fig. 4. As shown in Fig. 4a, it is observed that the tensile strength of the blends stayed nearly consistent. However, the elongation at break and the impact strength of the blends both increased firstly and then decreased, along with the increasing of the HBETP content, as shown in Fig. 4b. It indicates that the addition of an appropriate amount of HBETP can improve the toughness of the blends.

The improvement of the toughness lies in two factors. Firstly, HBETP contains a large amount of amino groups; whilst many hydroxyl groups and carboxyl groups exist within the PHBV and PBAT molecular chains. As a result, strong hydrogen bonding can be easily formed between HBETP and PHBV/PBAT. It enhances the physical entanglement and the interweaving between HBETP and the PLA/PBAT blends; Furthermore, an active terminal amino group

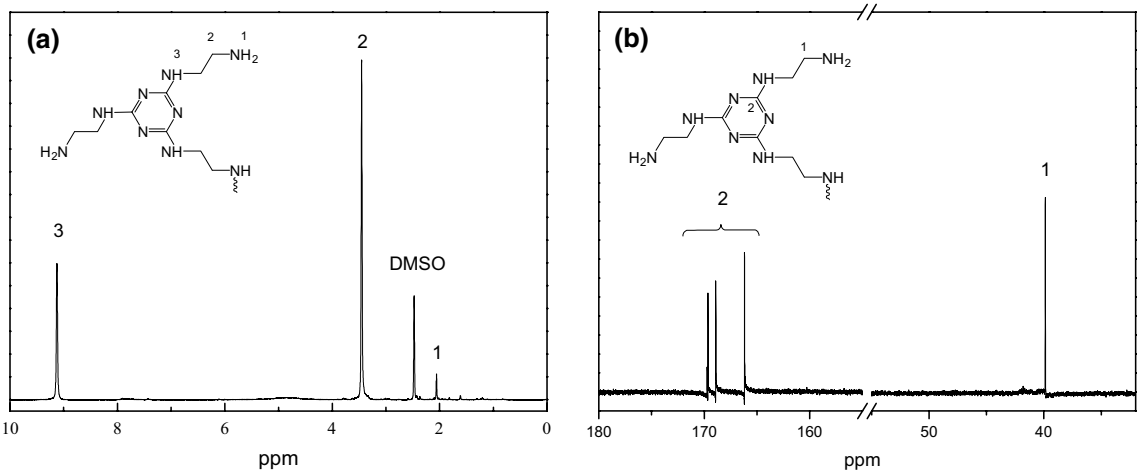

Fig. 3 ^{1}H-NMR (**a**) and ^{1}C-NMR (**b**) spectra of HBETP

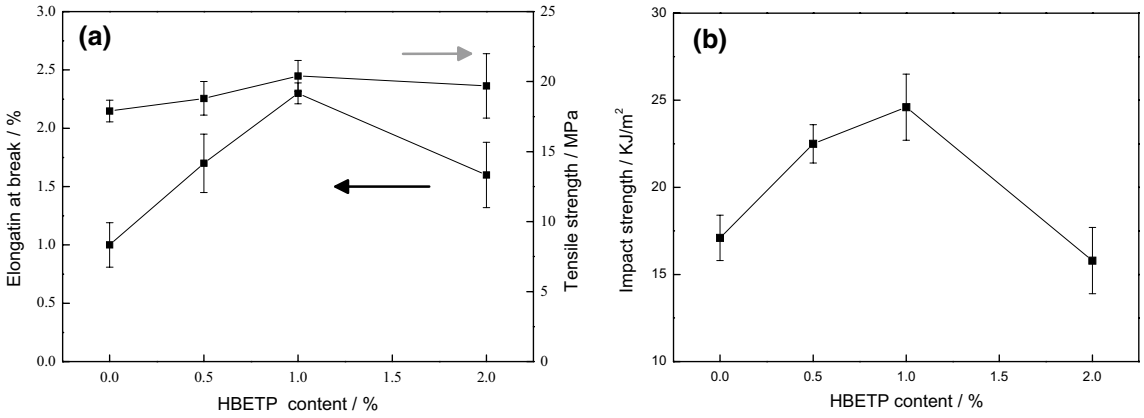

Fig. 4 **a** Tensile strength, elongation at break and **b** impact strength of the PHBV/PBAT blends with different contents of HBETP

of HBETP forms the amide bond with the carbonyl group of PHBV and/or PBAT (confirmed by XPS followed in "XPS Analysis of PHBV/PBAT" section), leading to a chemical micro-crosslinking between HBETP and the PHBV/PBAT blends.

The combined action of the strong physical hydrogen-bonding and the chemical micro-crosslinking makes the compatibility of PHBV and PBAT improved. The phase interface between PHBV and PBAT becomes no longer apparent, the size of the PBAT disperse phase in PHBV system is greatly reduced and the sea-island structure is almost disappeared. However, since there is only trace amount addition of HBTEP (< 2.0%), the completely melting miscibility at the molecular level cannot be achieved between PHBV and PBAT. The micro-phase separation still exists (confirmed by DMA and SEM followed in "SEM Analysis of PHBV/PBAT" and "DMA Analysis of PHBV/PBAT" sections). The presence of the micro-phase separation makes the tensile strength of the PHBV/PBAT system almost unchanged with different content of HBTEP.

Besides, the addition of HBETP in PHBV/PBAT can form a wider and more obvious gradient transition layer between PHBV and PBAT (see Fig. 5), which leads to the improvement of the compatibility between PHBV and PBAT. The inseparable gradient transition layer can quickly absorb the energy when impacted by external forces, which could dissipate the energy and subsequently increase the impact strength. Furthermore, it is well known that high generation of HBETP contains a large number of cavities inside (see Fig. 1). These cavities can also absorb the energy under external impact and thus give rise to the ulterior increase of the impact strength.

When the content of HBETP is 1.0 wt%, the impact strength of the blends reached the peak value, which is increased by 47.1% compared to that of the neat PHBV/PBAT. The reason of this phenomenon lies in: The combined action of the strong physical hydrogen-bonding and the chemical micro-crosslinking, especially the chemical micro-crosslinking, makes the structure of the PHBV/PBAT blends changed from linear structure to 3-D micro-crosslinked network structure. It helps the improvement of the elasticity and the impact strength of the blend system. When the HBETP content was less than 1.0%, the proper degree of crosslinking makes the impact strength of the PHBV/PBAT blends increased with the increase of HBETP content. When the content of HBETP was more than 1.0%, excessive micro-crosslinking restricts the movement and/or rotation of the molecular chain. At this point, the relative

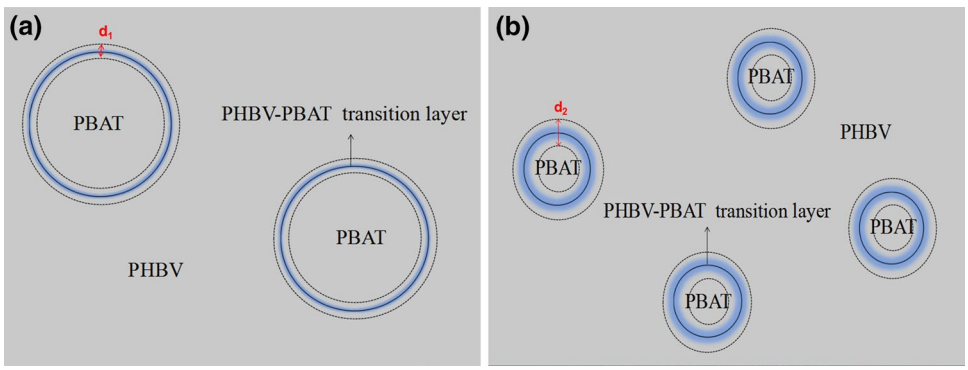

Fig. 5 The gradient transition layer diagram in PHBV/PBAT sea-island structure before (**a**) and after (**b**) proper addition of HBETP

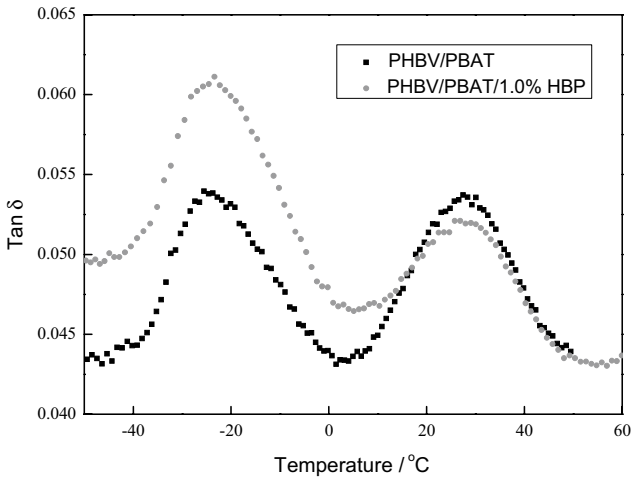

Fig. 6 DMA curves of the PHBV/PBAT blends before and after addition of 1.0 wt% of HBETP

Table 1 Thermal properties of the PHBV/PBAT blends before and after addition of 1.0 wt% of HBTEP obtained from DMA

HBTEP content (wt%)	T_{g1} (°C)	T_{g2} (°C)	ΔT_g (°C)
0	−24.8	28.4	53.2
1.0	−23.6	26.3	49.9

T_{g1} and T_{g2} are the glass transition points for PBAT and PHBV respectively

movement of the molecular chains is not feasible, only if the chemical bond is broken. Thus the impact strength is found decreased with the increasing of HBETP content.

DMA Analysis of PHBV/PBAT

As shown in Fig. 6, the PHBV/PBAT blends have two values of T_g, which correspond to T_g values of PHBV and PBAT, respectively. It indicates that PHBV and PBAT are thermodynamically incompatible with each other. After addition of HBETP, the DMA curve shows that the difference between two T_g values (ΔT_g) decreases (see Table 1 in detail). When the content of HBETP is 1.0 wt%, it is found that ΔT_g of the blends is 49.9 °C, which is 3.3 °C lower than that of the neat PHBV/PBAT blends.

It indicates that HBTEP is an excellent modifier which can improve the compatibility between PHBV and PBAT, but the complete melting miscibility at the molecular level cannot be achieved. The micro-phase separation between PHBV and PBAT still exists. However, the existence of micro-phase separation does not affect the toughening and modification results of HBP to PHBV/PBAT (see mechanical property results in "Mechanical Properties Analysis of PHBV/PBAT"). On the contrary, the existence of micro-phase separation contributes to the maintenance of a certain mechanical strength.

SEM Analysis of PHBV/PBAT

Figure 7 shows SEM images of the impact section of the blends. As shown in Fig. 7a, there are many pore and granular protrusions appeared in the matrix. Shape of the pore and the particle are regular and smooth, indicating the week interfacial adhesion between the two phases and the poor compatibility between the two substances. Upon addition of 0.5 wt% of HBETP, the cross-sectional island structure is not obvious. The protrusions and holes become smaller, as described in Fig. 7b. When the content of HBETP is 1.0 and 2.0 wt%, the island structures nearly disappear, as shown in Fig. 7c, d, respectively.

It must be noted that SEM can only provide the fractured morphology in micrometer level. Under this condition, it can be observed that the sea-island structure roughly disappeared. However, combined with the above DMA results, it concludes that the addition of HBETP cannot achieve the melting miscibility of PHBV and PBAT at the molecular level. The interface of the two phases still exists, which is consistent with the conclusions of DMA analysis above.

XPS Analysis of PHBV/PBAT

HBETP and HBETP modified PHBV/PBAT blends are characterized by XPS in order to confirm the formation of the amide bond between HBETP and the blends. The N 1s spectra of HBETP and HBETP modified PHBV/PBAT blends are shown in Fig. 8.

As expected, the N 1s spectrum of HBETP can be fitted with two components, N_{amino} and N_{C-N-C}, showing binding energy at 398.5 and 399.8 eV, which are consistent with those reported in literature [32]. A satisfactory fitting of the spectrum is carried out and shown in Fig. 8a.

On the other hand, as shown in Fig. 8b, in the N 1s spectrum of the HBETP modified blends, there are three types of nitrogen electronic environment observed. Apart from N_{amino} and N_{C-N-C}, a new component, $N_{O=C-N}$, showing binding energy at 400.8 eV [33, 34], can be assigned to the nitrogen atom within amide bond. The new formed $N_{O=C-N}$ component suggests the formation of the amide bond between terminal amino groups of HBETP and carbonyl groups in PLA and/or PBAT in blends.

XRD Analysis of PHBV/PBAT

Figure 9 represents the XRD patterns of the PHBV/PBAT blends. All diffraction planes are labeled. At first glance, there is no obvious change in terms of the number and the position of diffraction peaks, indicating that the addition of HBETP

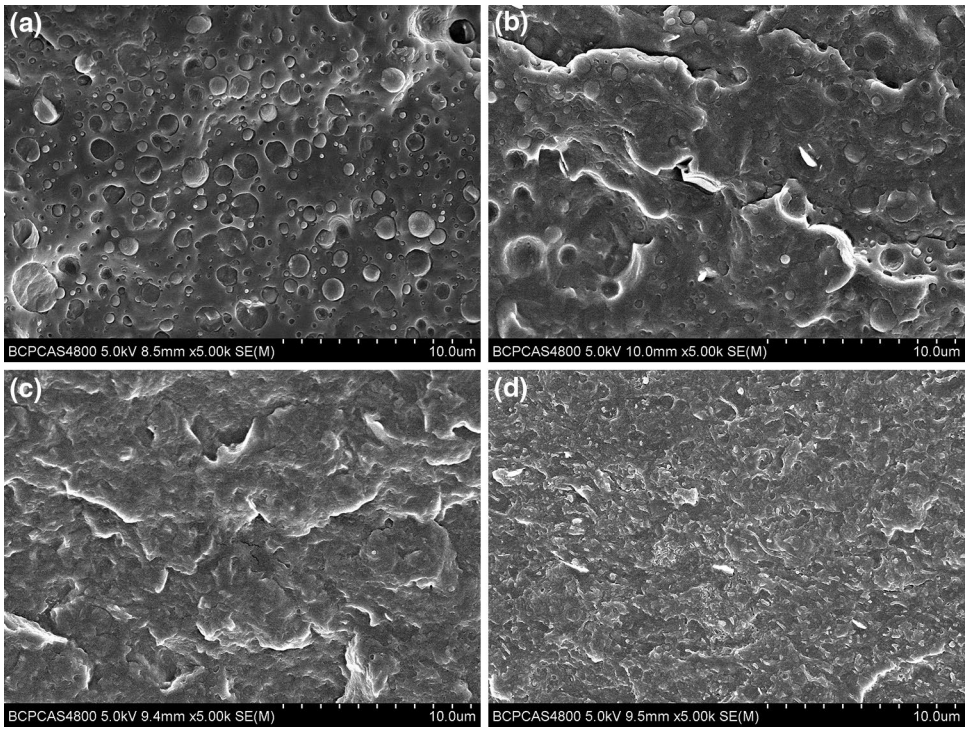

Fig. 7 SEM images of the PHBV/PBAT blends with different contents of HBETP: **a** 0 wt%, **b** 0.5 wt%, **c** 1.0 wt% and **d** 2.0 wt%

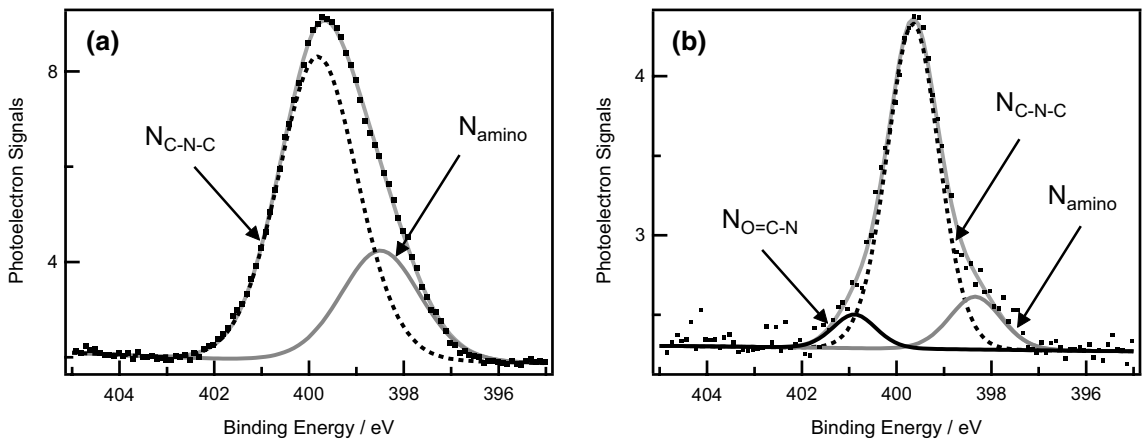

Fig. 8 N 1s high resolution spectra of HBETP and HBETP modified PHBV/PBAT blends

has no impact on the crystal shape, cell parameters and crystal structure of the blends. However, by carefully analyzing the XRD patterns, it is found that that with the increasing of HBETP content, progressive decrease of the intensity of (020), (101), (111), (040) and (200) planes has happened, indicating that the crystallinity of the blends is decreased. The crystallinity of all samples is calculated according to Eq. 1 and listed in Table 2.

$$Crystallinity = \frac{I_c}{I_c + I_a} \quad (1)$$

where I_c is the intensity of diffraction peak for the crystallized region; I_a is the one for amorphous region.

When the content of HBETP is 2.0 wt%, the calculated crystallinity is 34.8%, which is 24% lower than that of the neat PHBV/PBAT blends (see Table 2 in detail). It suggests that the addition of HBETP can limit the growth of the PHBV crystals.

(040) Plane is selected as a representative plane to show the change of the crystalline grain size of the sample. The calculation of grain sizes is conducted according to Eq. 2 and the results are also listed in Table 2. It is found that the grain size is decreased from 109.96 to 44.90 Å, which confirms that

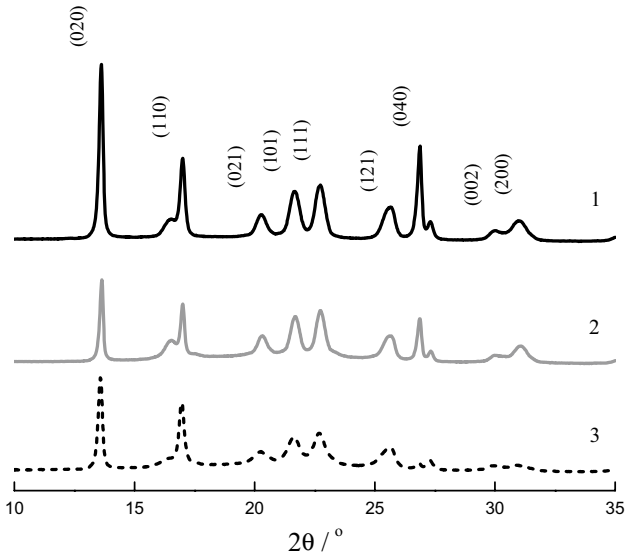

Fig. 9 XRD patterns of the PHBV/PBAT blends with different contents of HBETP. 1: 0 wt%, 2: 1.0 wt%, 3: 2.0 wt%

Table 2 Crystallinity of PHBV/PBAT blends with different contents of HBETP

HBETP content (%)	Crystallinity (%)	Intensity (040)	Grain size (040) (Å)
0	58.8	318.88	100.96
1.0	42.6	154.20	64.09
2.0	34.8	43.38	44.90

upon addition of HBTEP, the crystallinity and crystalline grain size of the blends are both reduced.

$$D = \frac{K\lambda}{\beta \cos\theta} \quad (2)$$

where D is the mean thickness of the grain perpendicular to the direction of the lattice plane; β represents the FWHM of the diffraction peak; λ is the wave length of X-ray; K is the Scherrer constant.

The XRD results conclude that the addition of HBETP can effectively reduce the crystallinity and the crystalline grain size of the blend system due to the formation of the transition layer between PHBV and PBAT.

DSC Analysis of PHBV/PBAT

DSC curves of the blends were recorded and shown in Fig. 10. The melting temperature and the crystallization temperature derived from DSC curves are also presented in Table 3.

As shown in Fig. 10a, it concludes that the crystallization temperature of the blends decreases from 96.77 to 91.44 °C, along with the increasing of the content of HBETP, which suggests that the crystallization of the blends becomes difficult upon addition of HBETP.

Furthermore, the splitting of the melting peaks upon addition of HBETP was more and more obvious, as demonstrated in Fig. 10b. In specific in the case of the blends with 2.0 wt% of HBETP, an unresolved doublet peak is observed.

It is well known that PHBV contains HV unit and HB unit, as shown in Fig. 1. The length of the side chain can significantly influence the flexibility of the molecular chain, and thus the orientation arrangement during crystallization. As a result, the crystallization of HV segment cannot be formed. However, the presence of HV segment can impact the crystallization of HB segment, leading to two HB crystalline regions. The one with higher melting temperature represents the HB crystalline region (T_{m2}); one with lower melting temperature is assigned to the HB-HV binary eutectic region (T_{m1}). The addition of HBETP helps to form the transition

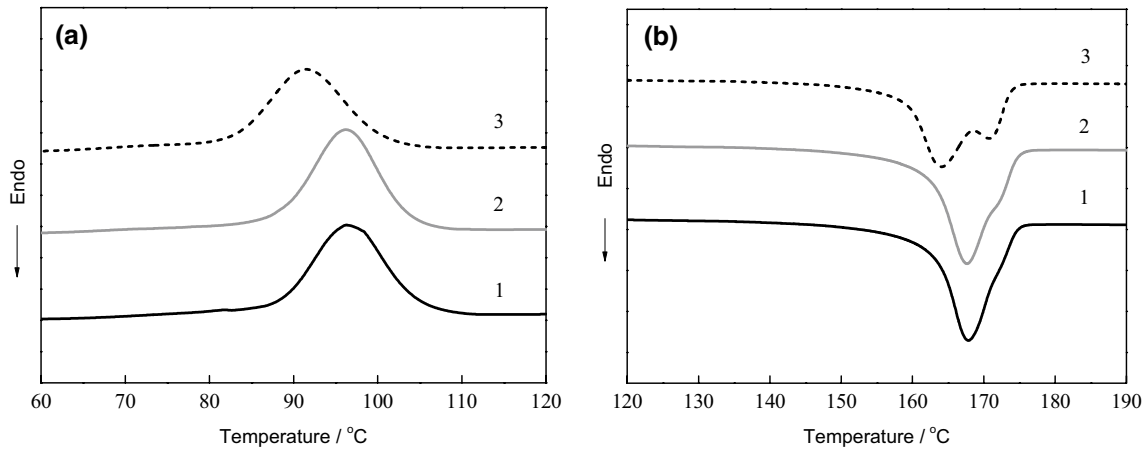

Fig. 10 DSC curves of the PHBV/PBAT blends with different contents of HBETP from the cooling (**a**) and heating (**b**) scans. 1: 0 wt%, 2: 1.0 wt%, 3: 2.0 wt%

Table 3 Thermal properties of the PHBV/PBAT blends with different contents of HBETP obtained from the cooling and heating scans

HBETP content (wt%)	T_{m1} (°C)	T_{m2} (°C)	T_c (°C)
0	168.14	172.93	96.77
1.0	167.62	172.25	96.13
2.0	164.02	171.07	91.44

T_{m1} represents the melting temperature of HB-HV binary eutectic region; T_{m2} corresponds to the melting temperature of the HB crystalline region

layer between PHBV and PBAT. It causes the moving of PBAT chain segment towards PHBV chain easier, which can preferentially affect the crystallization of the HB-HV binary eutectic region. With the increasing of the content of HBETP, such effect becomes more intense. When the content of HBETP is 2 wt%, T_{m1} is decreased by 4.1 °C (from 168.14 to 164.02 °C). It must be noted that T_{m2} is also decreased, with the increasing of the content of HBETP (from 172.93 to 171.07 °C). But such a decrease is not as obvious as that of T_{m1}, which confirms that the impact of the addition of HBETP upon crystallization of PHBV mainly focuses on the HB-HV binary eutectic region.

From another point of view, as has been claimed from XRD analysis, with the increasing of HBETP content, the crystalline grain size both decreased (see Table 2). The decrease of the crystalline size can cause the decrease of the melting temperature, meaning that the HB-HV binary eutectic region is partially changed to amorphous. The crystallinity decreases, which is consistent with the conclusion of XRD.

The decline of the melting temperature can not only reduce the energy consumption but also prevent the thermal decomposition of PHBV during processing. It helps to improve the processibility of PHBV.

Toughening Mechanism

The toughening mechanism of PHBV/PBAT modified by amino-terminated HBTEP dues to three reasons as follows which is shown in Fig. 11.

(1) Large numbers of terminal amino groups covering HBETP can cause strong hydrogen bonding effect and even the formation of amide bond, in the presence of the carboxyl groups and ester groups of PHBV and PBAT. Thus the entanglement and interweaving were

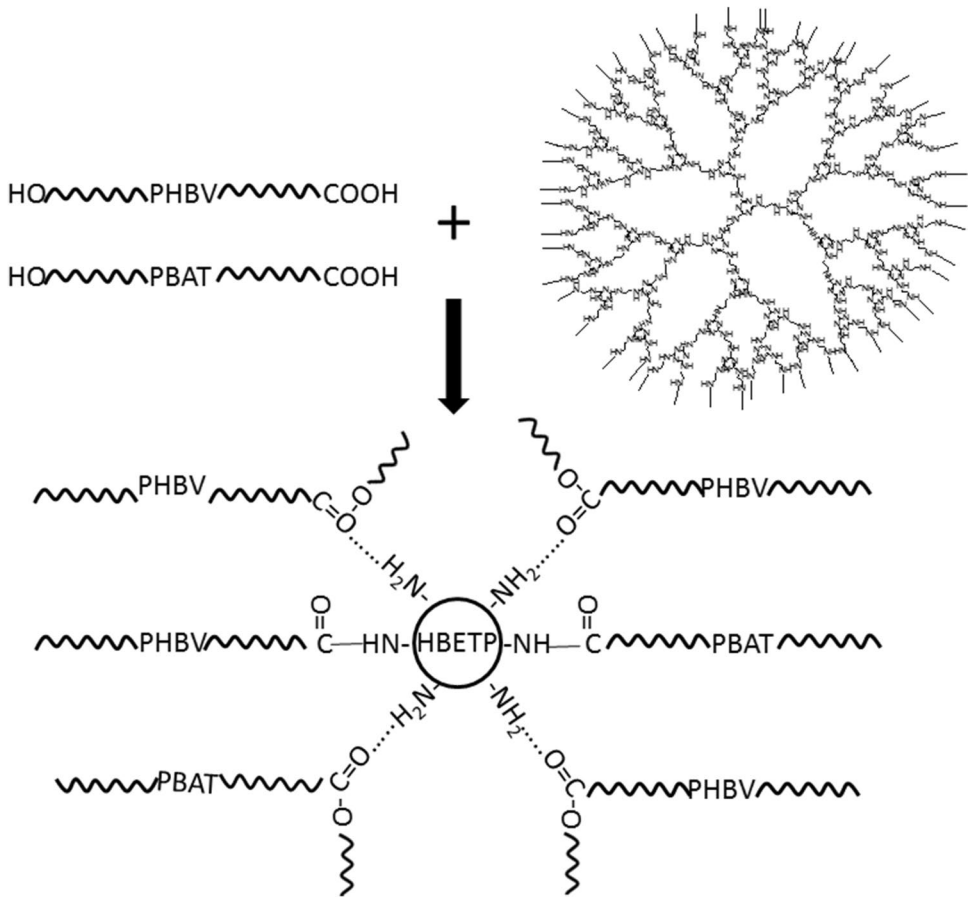

Fig. 11 Toughening mechanisms of the PHBV/PBAT blends modified by HBETP

strengthened between spherical HBETP and linear PHBV and PBAT. The gradient transition layer between PHBV and PBAT is formed, which can quickly absorb the energy under external impact, dissipate the energy and thus improve the impact strength.

(2) Strong hydrogen-bonding and chemical micro-crosslinking, especially the formation of chemically micro-crosslinked structures, can make the structure of the PHBV/PBAT blends changed from linear structure to 3-D micro-crosslinked network structure. It helps the improvement of the elasticity and the impact strength of the blend system.

(3) High generation of HBETP contains a large number of cavities inside which can also absorb energy under external impact and thus give rise to the ulterior increase of the impact strength.

Conclusions

A new synthesized amino-ended HBETP is used to modify the PHBV/PBAT blends. Upon addition of HBETP, properties of the blends are significantly improved. When the content of HBETP is 1.0 wt%, the impact strength of the blends is increased by 47.1%, compared to that of the neat blends, indicating that the toughness of the blends is enhanced. ΔT_g of the blends with 1.0 wt% of HBETP is found 3.3 °C smaller than that of the neat blends. SEM images on the fractured morphology of the blends also indicate that there is a transition layer between PHBV and PBAT formed. XRD results show that the addition of HBETP can effectively reduce the crystallinity and the crystalline grain size of PHBV. DSC results illustrate that the addition of HBETP can mainly influence the crystallization of the HB-HV binary eutectic region within PHBV. The toughening mechanism is discussed in detail. It suggests that both the hydrogen bonding effect and the formation of the amide bond occurred.

Acknowledgements The authors thank the National Nature Science Foundation (51503007), Support Project of High-level Teachers in Beijing Municipal Universities in the Period of 13th Five-year Plan (CIT&TCD201804030) and Beijing Municipal Natural Science Fund-Key project of science and technology plan of Beijing Education Committee (KZ201810011017) for financial support.

References

1. Weng Y, Wang L, Zhang M, Wang X, Wang Y (2013) Polym Test 32:60–70
2. Xing Z, Chae W, Baek J, Choi M, Jung Y, Kang I (2010) Biomacromolecules 11:1248–1253
3. Weng Y, Jin Y, Meng Q, Wang L, Zhang M, Wang Y (2013) Polym Test 32:918–926
4. Bledzki AK, Jaszkiewicz A (2010) Compos Sci Technol 70:1687–1696
5. Nanda MR, Misra M, Mohanty AK (2011) Macromol Mater Eng 296:719–728
6. Jin Y, Men S, Weng Y (2018) J Polym Eng 38:223–229
7. Kamiya N, Yamamoto Y, Inoue Y, Chûjô R (1989) Macromolecules 22:1676–1682
8. Sudesh K, Abe H, Doi Y (2000) Prog Polym Sci 25:1503–1555
9. Phua YJ, Pegoretti A, Araujo TM, Ishak ZAM (2015) J Appl Polym Sci 132:42815–42824
10. Javadi A, Kramschuster AJ, Pilla S, Lee J, Gong SQ, Turng LS (2010) Polym Eng Sci 50:1440–1448
11. Ten E, Turtle J, Bahr D, Jiang L, Wolcott M (2010) Polymer 51:2652–2660
12. Pawar SP, Misra A, Bose S, Chatterjee K, Mittal V (2015) Colloid Polym Sci 293:2921–2930
13. Nagarajan V, Misra M, Mohanty AK (2013) Ind Crop Prod 42:461–468
14. Bittmann B, Bouza R, Barral L, Castro-Lopez M, Dopico-Garcia S (2015) Polym Compos 36:2051–2058
15. Javadi A, Srithep Y, Lee J, Pilla S, Clemons C, Gong SQ, Turng LS (2010) Compos A 41:982–990
16. Cunha M, Fernandes B, Covas JA, Vicente AA, Hilliou L (2016) J Appl Polym Sci 133:42165
17. Resch-Fauster K, Klein A, Blees E, Feuchter M (2017) Polym Test 64:287–295
18. Jin YJ, Weng YX, Li XX, Zhang M, Xin XL (2015) J Mater Sci 50:794–800
19. Evstatiev M, Simeonova S, Friedrich K, Pei XQ, Formanek P (2013) J Mater Sci 48:6312–6330
20. Kumar M, Mohanty S, Nayak SK, Rahail Parvaiz M (2010) Bioresour Technol 101:8406–8415
21. Deng Y, Saucier-Sawyer JK, Hoimes CJ, Zhang J, Seo YE, Andrejecsk JW, Saltzman WM (2014) Biomaterials 35:6595–6602
22. Tang B, Liu X, Zhao X, Zhang J (2014) J Appl Polym Sci 131:40614
23. Fotiadou S, Karageorgaki C, Chrissopoulou K, Karatasos K, Tanis I, Tragoudaras D, Frick B, Anastasiadis SH (2013) Macromolecules 46:2842–2855
24. Luo L, Meng Y, Qiu T, Li X (2013) J Appl Polym Sci 130:1064–1073
25. Huber T, Pötschke P, Pompe G, Häßler R, Voit B, Grutke S, Gruber F (2000) Macromol Mater Eng 280–281:33–40
26. Zhou X, Zheng Q, Wang C, Xu J, Wu J, Kirk TB, Ma D, Xue W (2016) ACS Appl Mater Interfaces 8:12609–12619
27. Liu C, Yan H, Yuan L, Chen Z, Zhang M (2015) J Polym Sci Pol Chem 53:2132–2140
28. Houel A, Galy J, Charlot A, Gerard JF (2014) J Appl Polym Sci 131:1082–1090
29. Daraei P, Madaeni SS, Ghaemi N, Khadivi MA, Astinchap B, Moradian R (2013) J Membr Sci 444:184–191
30. Schüssele AC, Nübling F, Thomann Y, Carstensen O, Bauer G, Speck T, Mülhaupt R (2012) Macromol Mater Eng 297:411–419
31. Men S, Jiang J, Licence P (2017) Chem Phys Lett 674:86–89
32. Feng D, Zhou Z, Bo M (1995) Polym Degrad Stabil 50:65–70
33. Bar G, Rubin S, Cutts RW, Taylor TN, Zawodzinski TA (1996) Langmuir 12:1172–1179
34. Bakare RA, Bhan C, Raghavan D (2014) Biomacromolecules 15:423–435